Applying Advanced Ground-Based Remote Sensing in the Southeast Asian Maritime Continent to Characterize Regional Proficiencies in Smoke Transport Modeling

JAMES R. CAMPBELL,* CUI GE,+ JUN WANG,+ ELLSWORTH J. WELTON,# ANTHONY BUCHOLTZ,* EDWARD J. HYER,* ELIZABETH A. REID,* BOON NING CHEW,@ SOO-CHIN LIEW,@ SANTO V. SALINAS,@ SIMONE LOLLI,& KATHLEEN C. KAKU,** PENG LYNCH,** MASTURA MAHMUD,++ MAZNORIZAN MOHAMAD,## AND BRENT N. HOLBEN#

* *Naval Research Laboratory, Monterey, California*
+ *Department of Atmospheric Sciences, University of Nebraska–Lincoln, Lincoln, Nebraska*
# *NASA Goddard Space Flight Center, Greenbelt, Maryland*
@ *Centre for Remote Imaging Sensing and Processing, National University of Singapore, Singapore*
& *Joint Center for Earth Systems Technology, Greenbelt, Maryland*
** *Computer Sciences Corporation, Monterey, California*
++ *National University of Malaysia, Bangi, Selangor, Malaysia*
Environmental Studies Division, Malaysian Meteorological Department, Petaling Jaya, Selangor, Malaysia

(Manuscript received 19 March 2015, in final form 12 August 2015)

ABSTRACT

This work describes some of the most extensive ground-based observations of the aerosol profile collected in Southeast Asia to date, highlighting the challenges in simulating these observations with a mesoscale perspective. An 84-h WRF Model coupled with chemistry (WRF-Chem) mesoscale simulation of smoke particle transport at Kuching, Malaysia, in the southern Maritime Continent of Southeast Asia is evaluated relative to a unique collection of continuous ground-based lidar, sun photometer, and 4-h radiosonde profiling. The period was marked by relatively dry conditions, allowing smoke layers transported to the site unperturbed by wet deposition to be common regionally. The model depiction is reasonable overall. Core thermodynamics, including land/sea-breeze structure, are well resolved. Total model smoke extinction and, by proxy, mass concentration are low relative to observation. Smoke emissions source products are likely low because of undersampling of fires in infrared sun-synchronous satellite products, which is exacerbated regionally by endemic low-level cloud cover. Differences are identified between the model mass profile and the lidar profile, particularly during periods of afternoon convective mixing. A static smoke mass injection height parameterized for this study potentially influences this result. The model does not resolve the convective mixing of aerosol particles into the lower free troposphere or the enhancement of near-surface extinction from nighttime cooling and hygroscopic effects.

1. Introduction

Advances in tropospheric aerosol mass transport modeling over the last decade are a reflection of two primary influences: the maturation of operational and research-grade modeling systems themselves (e.g., Grell et al. 2005; Wang et al. 2006; Lohmann et al. 2007; Hollingsworth et al. 2008; Benedetti et al. 2009; Colarco et al. 2010; Zhang et al. 2008, 2011, 2014) and the rapid accumulation of available source characterization datasets from the many satellite remote sensors launched during the period (e.g., Anderson et al. 2005; Zhang and Reid 2006; Li et al. 2009; Reid et al. 2009; Hyer et al. 2011; Shi et al. 2011). Accordingly, increasing model skill has been achieved over a host of significant aerosol–climate processes, including the resolving of aerosol particle scattering profiles and regional distributions necessary for analysis of trends (Zhang and Reid 2010), assessments of visibility/hazards (e.g., Langmann et al. 2012; O'Dowd et al. 2012), and evaluating their aerosol radiative impact on climate (e.g., Pérez et al. 2006; Ghan and Schwartz 2007; Chapman et al. 2009; Koffi et al. 2012). Furthermore, gains have been made over all

Corresponding author address: James R. Campbell, c/o Naval Research Laboratory, 7 Grace Hopper Ave. Stop 2, Monterey, CA 93943.
E-mail: james.campbell@nrlmry.navy.mil

DOI: 10.1175/JAMC-D-15-0083.1

relevant spatial scales, including urban (e.g., Banta et al. 2005; Wong et al. 2015), mesoscale (e.g., Wang and Christopher 2006; Wang et al. 2006), synoptic (e.g., Song et al. 2008; Magi et al. 2009), and global domains (e.g., Chin et al. 2002; Zhang 2013).

At progressively finer transport scales, an evaluation of model efficacies becomes more challenging, since processes involving aerosol particle source generation, lofting, microphysical/chemical evolution, and downwind dispersion are increasingly significant at finer scales, interacting in more complex ways (Anderson et al. 2003). For instance, with a global transport model, column-integrated mass concentrations, and/or their use as first-order proxies for aerosol optical depth (AOD), are reasonable dependent model parameters for assessing analytical and predictive skill (Zhang et al. 2008; Morcrette et al. 2009). Less concern is thus given to the performance of underlying model dynamics, complexity of source composition partitioning, numerical diffusion effects, and mass deposition budgeting (Xian et al. 2009). At sufficiently broad scales, these are second- and third-order concerns to the system developer. Model complexity, as it impacts overall skill, is thus most commonly inversely proportional to scale. Consequently, complex treatments of aerosol composition and processing in global models have resulted in verification results little or no better than relatively coarse approaches (e.g., Kinne et al. 2005). The verification of finer-scale model transport performance requires datasets, accordingly, that match their high corresponding spatial and temporal resolutions, particularly where observational densities, both from ground and satellite, are low.

Scale aside, the remote sensing community faces fundamental obstacles collecting representative datasets for meaningful model evaluation and innovation, transport based or otherwise. Though the information content (i.e., diversity and accuracy) available from synergistic surface-based and satellite remote sensing frequently satisfies both goals (e.g., Colarco et al. 2004), limits remain in what is practically observable and actually measureable. For instance, polar-orbiting satellite-based sensors are limited by coverage and sampling issues (e.g., Holz et al. 2008; Colarco et al. 2014). Similarly, it can be a logistical nightmare deploying sufficient ground-based instrumentation into regions of interest for any significant length of time. It can be equally challenging isolating specific aerosol types during transport as well for straightforward model evaluation, given the propensity for air mass mixing downwind that complicates scene characterization (e.g., Ansmann et al. 2009).

On 25–28 September 2012, the Naval Research Laboratory (NRL), NASA Micro-Pulse Lidar Network (MPLNET; Welton et al. 2001), and NASA Aerosol Robotic Network (AERONET; Holben et al. 1998) conducted an 84-h intensive field study at Kuching, Malaysia [1.49°N, 110.35°E; 0.028 km above mean sea level (MSL)], during relatively dry conditions, that was designed specifically for the physical and thermodynamic evaluation of a mesoscale smoke transport model. The period coincided with significant near-surface particle loading almost exclusively attributable to local and regional (approximately 300–500 km upwind, or 1–2 days) transport of anthropogenic biomass burning residues (Fig. 1). Instruments operated at the site included a continuously running ground-based 355-nm polarization-sensitive atmospheric lidar system (ALS; Lolli et al. 2011) and a multiwavelength sun photometer. Further, as the site was located on the grounds of the Malaysian Meteorological Department (MMD) station at the Kuching International Airport, radiosonde profiles were collected every 4 h. This featured both operational 12-hourly (0000 and 1200 UTC) profiles, consistent with World Meteorological Organization (WMO) protocols (http://www.wmo.int/pages/prog/www/ois/volume-a/vola-home.htm), and supplemental ones (0400, 0800, 1600 and 2000 UTC). During the 84 h from 0000 UTC 25 September through 1200 UTC 28 September, 22 consecutive 4-hourly thermodynamic profiles, including winds, were collected.

Simulating and forecasting potentially hazardous aerosol particle outbreaks for high-density urban areas in Southeast Asia (SEA)/the "Maritime Continent" (MC) represent a primary objective for local meteorological agencies and research groups. The region is, in particular, inundated by anthropogenic smoke during summer monsoonal months. However, it is difficult to routinely monitor regional conditions from satellite because of endemic cloud cover, limiting satellites' utility as both assimilation and verification data sources. Thus, the motivation for this study is based on applying the unique NRL/MPLNET/AERONET in situ smoke dataset for evaluating the proficiency of a state-of-the-art mesoscale aerosol model in resolving a relatively uncomplicated regional smoke transport event at this remote tropical site. The goal is to compare model depictions of smoke distribution and optical properties with the lidar/sun photometer, and model thermodynamic parameters and wind fields with high-resolution radiosonde data, to evaluate overall model efficacies.

Note that this research is specifically not designed for evaluating model sensitivities to physical parameterization, boundary conditions, and other inputs. That work is outside the current focus and is instead the basis

FIG. 1. Picture taken 1800 LT 26 Sep 2012 approximately 2 km northwest of the MMD field site (building with tower on upper left) at the Kuching International Airport (the runway field is apparent in the distance; approximate distances are denoted), depicting the optical density of the near-surface smoke present during the 84-h data collection period described. The first/short hill seen just beyond the center of the airport is approximately 6 km from the observer, and the larger hill whose faint outline is apparent was roughly 9 km away (the photograph was taken by author JRC).

for continuing research in the region (e.g., Wang et al. 2013; Ge et al. 2014). Known limitations within the modeling system and its essential parameterizations are identified, and a qualitative assessment of model skill in depicting significant aerosol features with respect to thermal evolution of the near-surface convective mixed layer and local sea breeze is summarized. The emphasis of this paper is on the unique capabilities of the observational dataset for the purposes of evaluating transport model performance. Careful examination of this case study using the detailed datasets collected in situ show where current proficiencies stand, given a reasonable and consistent set of system inputs, and thus where model development efforts should be directed.

2. Experimental factors

a. Background

Southeast Asia and western portions of the surrounding archipelago, referred to colloquially as the Maritime Continent, represent an unusually compelling natural laboratory environment for studying, and thus modeling, biomass burning processes [the recent review by Reid et al. (2013) outlines the scientific questions and observational challenges of studying aerosol processes in the region]. The southern MC is inundated by fires on all scales during its dry summer monsoonal period (roughly July–November), as farmers conduct annual clearing of what are mostly peat lands and low-lying brush (Fuller and Murphy 2006; Miettinen and Liew 2009, 2010; Miettinen et al. 2011; Reid et al. 2012). With relatively high carbon content, peat fires, for instance, correspond with significant transboundary smoke production (Page et al. 2002; Miettinen et al. 2011). Yet regional SEA/MC emissions plumes are constrained to relatively shallow depths, with climatological mean scattering profiles at visible wavelengths exhibiting little significant particle mass above roughly 3 km MSL over land (Campbell et al. 2013; Chew et al. 2013). This enhances the risk of surface exposure and deposition during transport, and seasonal burning is now recognized as a substantial threat to regional air and environmental quality (See et al. 2006; Salinas et al. 2009; Hyer and Chew 2010; Salinas et al. 2013).

Kuching is located in the northwest corner of Borneo, the third largest island in the world, which includes Brunei to the northwest, the Malaysian provinces of Sarawak and Sabah to the north, and the Indonesian provinces of North, West, East, Central and South

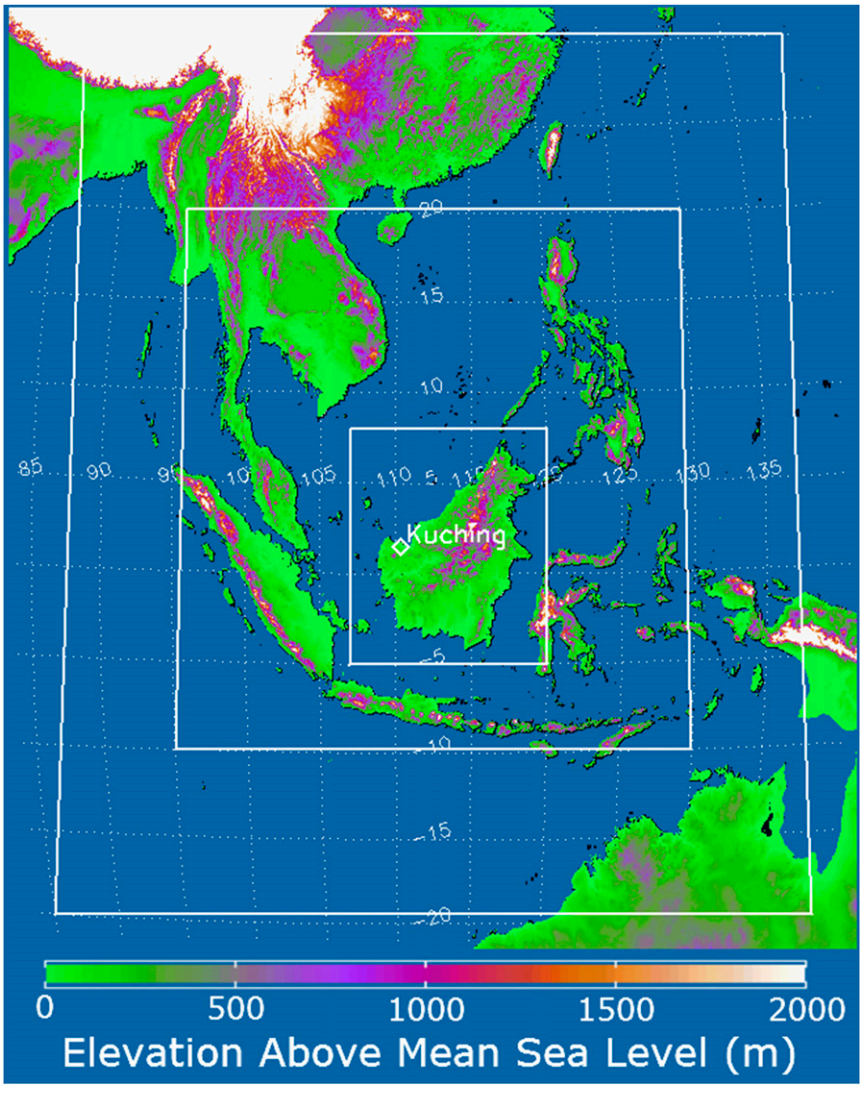

FIG. 2. Topographical map (m MSL) of Southeast Asia and the Maritime Continent. The WRF-Chem 81-km^2 nested domain is encapsulated by 20°S–30°N and 85°–140°E. The regional 27-km^2 nest is bound by 10°S–20°N and 95°–130°E. The final mesoscale 9-km^2 nest is bounded by 5°S–8°N and 107°–120°E so as to encapsulate the island of Borneo. Each domain is highlighted, with the Kuching MMD site further denoted.

Kalimantan to the south. The city is displaced roughly 50 km inland from the southern shores of the South China Sea (SCS; Fig. 2). Borneo itself features a distinct mountainous chain, reaching from the west-central portion of the island to its northeast, with the highest peaks near 2.0 km. Relatively flat plains surround the central mountains, including Kuching and most of the far-western portion of the island that is relatively devoid of significant topography. Freshwater and peat swamp forests exist along the western, southwestern, and southern coastlines, which are vulnerable to deforestation and clearing for agricultural conversion (Langner et al. 2007; Sarvision 2011). As will be described, fires generated along this periphery of the island proved the likeliest sources for upwind smoke propagation (~200–500 km) over northwestern Borneo during the period of intensive data collection. Kuching thus acts as a primary receptor site for smoke in a south-southwesterly flow, combined with the density and frequency of fires in southern and western Borneo during the summer monsoonal period (e.g., Mahmud 2009, 2013; Hyer et al. 2013).

b. *Regional weather conditions*

Data collected on 25–28 September at Kuching were unique in one critical respect for monitoring aerosol

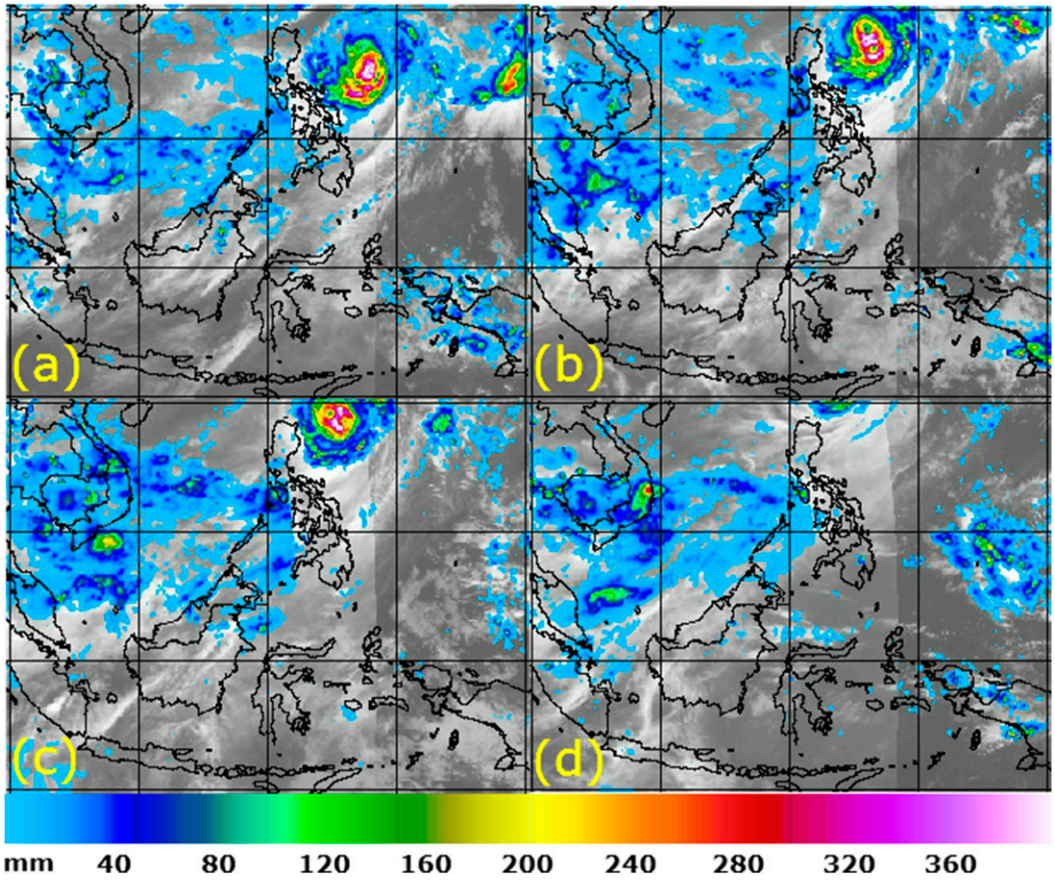

FIG. 3. Multisatellite blended retrievals of daily precipitation totals (mm) over SEA/MC for (a)–(d) 25–28 Sep 2012.

particle transport, particularly in Southeast Asia: effectively no precipitation fell during the 84-h data collection period. Despite what were relatively dry summer monsoonal conditions, which peak locally in July, Kuching still experiences over 200 mm of monthly averaged precipitation during September. Shown in Fig. 3 are blended multisatellite daily precipitation composites (Turk and Miller 2005; Turk and Xian 2013) for SEA/MC on each respective day. No precipitation was detected over northwestern Borneo on any of the four days by satellite estimation. A trace of rainfall was observed at Kuching from a passing convective cell on the afternoon of 26 September (Kuching local time = UTC+0800), as will be inferred from the lidar composites below. Conspicuously, a tropical cyclone (TC) was passing north of the Philippines. Reid et al. (2013) note the correlation between relatively broad regional subsidence and sustained southwesterly storm inflow within the MC during periods of TC activity to the north, which reconciles well with conditions experienced during this period. Consequently, aside from optical observing conditions from the ground, transport over the 84-h period would have occurred effectively unperturbed by wet deposition.

Despite the lack of any significant precipitation, however, the period was marked by a persistent and optically dense cirrus cloud shield over the site, limiting satellite and complicating passive ground-based observations. An example of this is shown in Fig. 4 for 26 September, taken from the NASA Moderate Resolution Infrared Spectroradiometer (MODIS; King et al. 2003), aboard the *Aqua* satellite, and the Cloud–Aerosol Lidar with Orthogonal Polarization (CALIOP) instrument aboard the *Cloud–Aerosol Lidar and Infrared Pathfinder Satellite Observations* (*CALIPSO*) platform; Winker et al. 2010). The two instruments are flown in sequence in the NASA A-Train constellation (e.g., Stephens et al. 2002). The MODIS true-color composite image (Fig. 4a) reflects the 0550 UTC afternoon overpass. However, the CALIOP level 1 attenuated backscatter data shown ($km^{-1}\,sr^{-1}$; Fig. 4b) and corresponding superimposed ground track in Fig. 4a reflect the nighttime pass later that day (beginning 1815 UTC, from north to south), which was the closest CALIOP overpass to Kuching during the 84-h sequence.

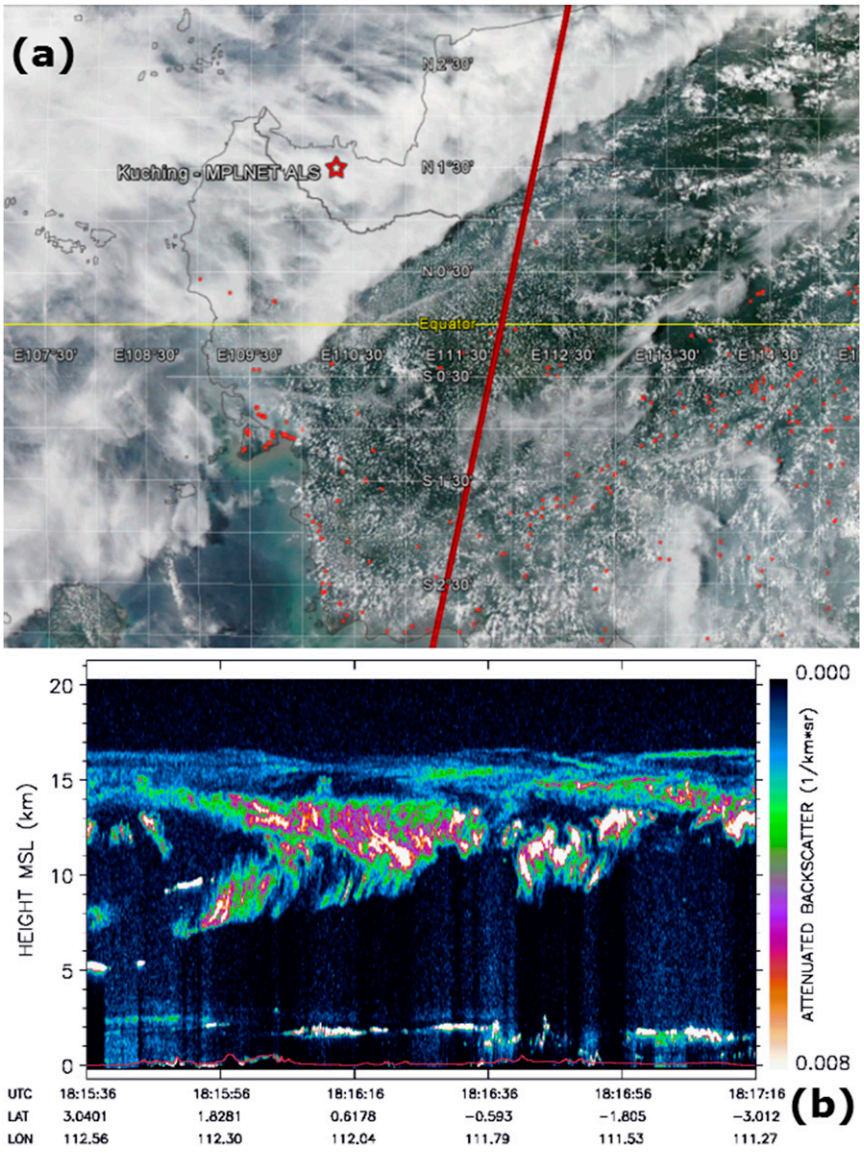

FIG. 4. (a) *Aqua* MODIS true-color composite from 0550 UTC 26 Sep 2012 over northwestern Borneo. Active fires observed by MODIS algorithms are superimposed in red. The Kuching MMD site is denoted, as is the corresponding CALIOP ground track (nighttime; from north to south) beginning 1815 UTC 26 Sep 2012 and corresponding to (b) the attenuated backscatter ($km^{-1}\,sr^{-1}$) measured from 0 to 20 km MSL, with surface altitude superimposed.

A dense shroud of cirrus clouds was present over northern Borneo, as observed from MODIS. CALIOP profiling helps distinguish the relatively deep cloud layers for anvil blow off near and below the approximate level of neutral convective buoyancy regionally around 14.5 km (Gettelman and Forster 2002) from tropical tropopause cirrus formed within a tropopause transition layer above to near 17.0 km (McFarquhar et al. 2000; Gettelman et al. 2004; Jensen et al. 2007). Cloud was persistent at both levels throughout the 84-h period.

AERONET (http://aeronet.gsfc.nasa.gov/) sun photometer level 1.0 spectral decomposition algorithm retrievals (O'Neill et al. 2003) of total, fine-, and coarse-mode AOD are shown from Kuching for 25–28 September in Fig. 5. Level 1.0 data, prior to quality assurance and including only basic first-order cloud screening, are specifically shown here qualitatively so as to depict the variability in coarse-mode and total AOD versus the relative stability in fine-mode values. The coarse-mode optical depths are sensitive to larger cirrus ice crystal scattering (when unscreened), whereas the fine-mode

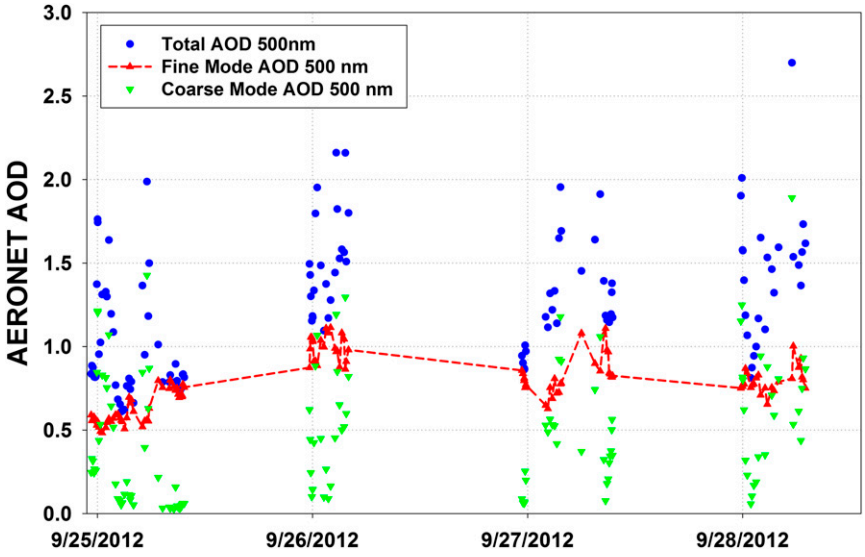

FIG. 5. AERONET level 1.0 spectral decomposition algorithm (see text) retrievals of total (blue circles), fine- (red upward triangles and connecting line), and coarse-mode (green downward triangles) AODs at 500 nm for 25–28 Sep 2012 at the Kuching MMD site (corresponding fractional days 269–272).

optical depths are sensitive to relatively smaller particles attributable to smoke and are mostly insensitive to cirrus cloud particles. The relatively persistent nature of the smoke observed at Kuching during this period thus stands out in the fine-mode response, in contrast to the comparatively erratic distribution of cirrus overhead, with AOD values generally between 0.5 and 1.0 that peak on 26 and 27 September. This detailed analysis of the height and composition of particle layers in cases of mixed cloud cover and smoke aerosols is only possible using the novel lidar/sun photometer combination deployed in this experiment.

c. *Processing of Kuching ALS measurements*

ALS measurements at Kuching were collected by MPLNET (http://mplnet.gsfc.nasa.gov/) during August and September 2012. Of note here, however, are solutions for the 355-nm aerosol particle extinction coefficient (km^{-1}) that are generated from attenuated backscatter ($km^{-1}\,sr^{-1}$) profiles solved after calibrating normalized signal returns recorded by the instrument at 75-m vertical and 1-min temporal sampling resolutions. The extinction coefficient and its uncertainty are solved, after clearing the data for low-level cloudy profiles that directly impact the aerosol profile, using an a priori estimate of the ratio for lidar extinction and backscatter coefficients, the so-called lidar ratio, to process those aerosol particle signals identified. ALS optical overlap is complete at approximately 300-m range, making it relatively well suited for aerosol profiling (Lolli et al. 2011). This assumption helps constrain the equation for elastic-scattering single-wavelength lidar measurements, which otherwise reflects a single equation with these two distinct unknown values (Fernald 1984). A static value was chosen here, 60 ± 10 sr, to represent smoke. This is a reasonable setting, compared both with estimates in the literature for lidar ratios derived for smoke using ultraviolet wavelength lidars (e.g., Balis et al. 2003; Müller et al. 2005; Noh et al. 2007) and tuning of integrated ALS column extinction (i.e., AOD) versus fine-mode 355- and 500-nm AERONET AOD (Fig. 5).

d. *WRF-Chem system design and model parameterizations*

Version 3.5.1 of the online-coupled WRF Model coupled with chemistry (WRF-Chem) is used to simulate mesoscale smoke transport within the SEA/MC domain. Recently, Wang et al. (2013) and Ge et al. (2014) used an older version of the model to study the impact of local land/sea breeze, typhoon, and topographic effects on the regional distribution of transported smoke and its vertical radiative heating profile. Here, a series of nested domains are constructed to conduct the simulations (Fig. 2). National Centers for Environmental Prediction Final Analysis (FNL; http://rda.ucar.edu/datasets/ds083.2/) 1° × 1° global meteorological datasets at 0000, 0600, 1200, and 1800 UTC are applied to initialize lateral boundary conditions along the outer 81-km-resolution regional nest. A 27-km-resolution local grid then surrounds a 9-km-resolution mesoscale one—the latter designed to encompass all of Borneo with the highest available horizontal resolution

(Fig. 2). FNL data are assimilated each time step at every nested model grid point using four-dimensional data assimilation and nudging of temperature, water vapor, and wind fields (Stauffer and Seaman 1994; Liu et al. 2008). Two-way model exchange between all nests is allowed. A terrain-following hydrostatic pressure coordinate system is used featuring 49 vertical levels, of which 25 are within the first 4 km above ground. The model was spun up for 10 days prior to 25 September in order for the background model aerosol fields to equilibrate. Table 1 lists all relevant physical parameterizations used, which are described and justified in further detail by Wang et al. (2013) and Ge et al. (2014). The model simulation includes parameterizations to account for land/sea surface interaction, cloud and aerosol radiative coupling, cloud microphysics and cumulus development, gas-phase and aerosol chemistry, and wet deposition.

All fire sources on Borneo are resolved within the finescale grid using NRL Fire Locating and Modeling of Burning Emissions (FLAMBE; Reid et al. 2009) datasets (http://www.nrlmry.navy.mil/aerosol_web/7seas/7seas.html), which are based on MODIS fire radiative power products. In turn, FLAMBE detections here reflect only those fires resolved with the two (*Aqua* or *Terra*) MODIS sensors, leaving four potential passes over Borneo each day. Reid et al. (2009) describe how such data are adapted for generating a diurnal emissions product. Here, hourly emissions are calculated using a fire diurnal cycle based on climatology of geostationary fire observations. Analysis of diurnal emissions cycles for this region (Hyer et al. 2013) indicates that the late morning/early afternoon overpass times of MODIS are a source of low bias in emissions from many types of fires in this region, but no quantitative correction for this effect is attempted here. Injection of smoke emissions within the model follows Wang et al. (2013) and occurs at 800 m MSL, a static level derived from comparison between regional simulations and seasonal CALIOP climatological scattering profiles. A two-day maximum (previous day and present day) fire signal is used to minimize orbital-limitation effects, in which the fire signal may be missed because of the limits of orbital coverage or cloud cover. This correction thus presumes a self-sustained nature to the fires, which is comparable with other current fire emissions products (e.g., Mu et al. 2011; Wiedinmyer et al. 2011). The ratio for organic-to-black carbon (OC/BC) is set to a constant 10, with size distributions for both represented in an accumulation mode with volume mean diameter of 0.3 μm and standard deviation of 2.0 (Ge et al. 2014).

TABLE 1. Model configuration options chosen for WRF-Chem in this study.

Atmospheric process	Model option
Surface layer	MM5
Land surface	Noah
Boundary layer	Yonsei University (YSU; Hong 2006)
Cumulus clouds	Grell ensemble cumulus scheme (G3; Grell and Devenyi 2002)
Cloud microphysics	Lin (Lin et al. 1983)
Gas-phase chemistry	Regional Acid Deposition Model, version 2 (RADM2; Stockwell et al. 1990)
Aerosol chemistry	MADE/SORGAM (Ackermann et al. 1998; Schell et al. 2001).
Horizontal resolution	Inner nested domain: 9 km × 9 km Regional nested domain: 27 km × 27 km Outer synoptic nested domain: 81 km × 81 km
Emission	FLAMBE, INTEX-B, dust, sea salt

Biogenic land surface source emissions [i.e., soil NO_x and volatile organic compounds (VOC)] are calculated using the Guenther et al. (1994) method, and sea salt and dust (Ackermann et al. 1998; Schell et al. 2001) are calculated within the Modal Aerosol Dynamics Model for Europe (MADE)/Secondary Organic Aerosol Model (SORGAM). Dust, however, is not explicitly considered as output here. This is not necessarily a poor assumption in SEA/MC, however, considering the focus here on near-surface smoke advection and that dust observed locally typically corresponds to long-range transport observed in the lower-to-middle free troposphere (e.g., Campbell et al. 2013). Anthropogenic emissions from SEA/MC are obtained from 2006 Intercontinental Chemical Transport Experiment (INTEX-B) estimates (Zhang et al. 2009), which include SO_2, NO_x, CO, VOC, particles of diameter less than 10 (PM10) and 2.5 μm (PM2.5), BC, and OC by sector (power, industry, residential, and transportation) and six speciated VOCs by sector files. Corresponding emissions in nearby regions (e.g., northern Australia) are adopted from Goddard Chemistry Aerosol Radiation and Transport (GOCART) model global emissions (Chin et al. 2002), which include source estimates for SO_2, BC, and OC. Specifically, sulfates are used as a proxy for all pollution aerosols.

3. Observations at Kuching

Shown in Fig. 6 are 0000 and 1200 UTC 96-h back trajectories, derived from the Hybrid Single-Particle Lagrangian Integrated Trajectory (HYSPLIT) model (Draxler and Rolph 2013) from 0000 UTC 25 September

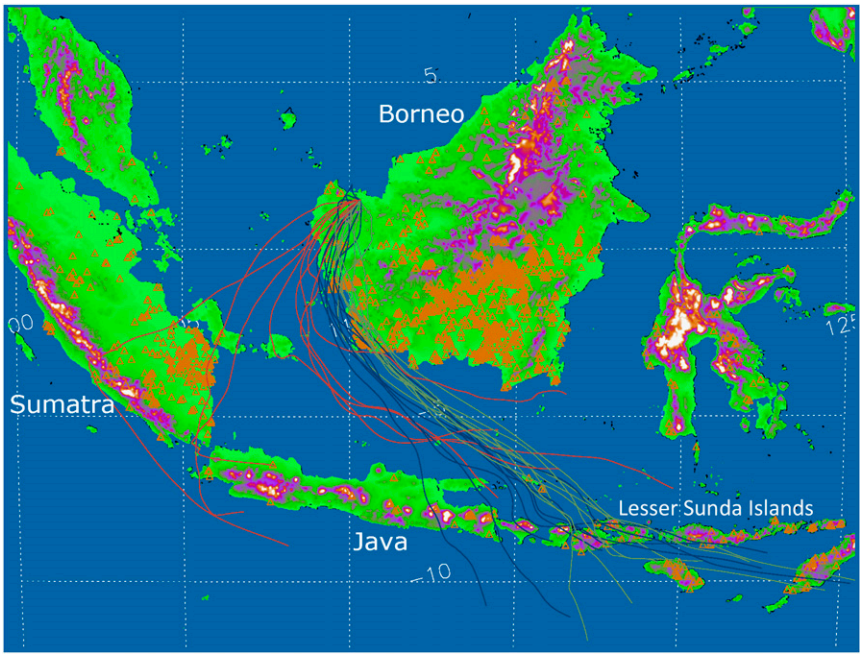

FIG. 6. The 96-h HYSPLIT back trajectories beginning from the Kuching MMD site at 500 (blue), 1500 (gray), and 2500 m MSL (red) for 0000 and 1200 UTC each day 25–28 Sep 2012. All fires identified with *Terra* and *Aqua* MODIS during this period are denoted by orange triangles. Ground topography is again superimposed, with a scale as in Fig. 2.

to 1200 UTC 28 September, beginning from the Kuching MMD site. Three sets of profiles are shown: 500, 1500, and 2500 m MSL. Superimposed on these data are all fires identified using *Terra* and *Aqua* MODIS during the 84-h measurement period. Topography is further superimposed, following Fig. 2.

Low-level flow during the period was relatively well concentrated along the southwestern Borneo coastline. There, two areas of persistent fire activity were observed: one along the central coast and another along the far-southwestern coast. Back trajectories at 500 and 1500 m MSL all intersect these regions, and/or within 50 km of them, reaching back to the Lesser Sunda Islands east of Java. Flow ending at 2500 m MSL at Kuching was variable, in contrast, mostly displaced west of these fires, though still near the western coast of the island. Some of these trajectories reach as far west as Sumatra, where active fires were also observed, and northwestern Java. This circulatory regime contrasts with conditions described, for instance, by Reid et al. (2013) and Wang et al. (2013) from case studies in 2006 across western Borneo and the Java Sea. It is consistent, however, with the seasonal likelihood for smoke transport trajectories originating over Java and the Lesser Sunda Islands that year described by Xian et al. (2013). Varying Madden–Julian oscillation and El Niño–Southern Oscillation (ENSO) phases exert overwhelming influences on what often prove to be varying regional circulatory features.

Shown in Fig. 7 are cloud-cleared (note some missing data because of cloud contamination) 355-nm aerosol extinction coefficients (km^{-1}) solved by MPLNET for ALS data collected, again, from 0000 UTC 25 September to 1200 UTC 28 September at the Kuching MMD site. Superimposed on these data are virtual potential temperature isotherms (VPT; 1-K increments) and water vapor mixing ratio contours ($g\,kg^{-1}$) solved at 25-m vertical resolution from the 4-hourly radiosonde profiles. Relatively dense aerosol particle layers are persistent through the period, confined mostly to within 3.0 km of the surface overall, which is consistent with regional climatology (Campbell et al. 2013).

There are multiple noteworthy features apparent with respect to aerosol particle loading and stratification relative to the corresponding thermodynamic environment. Working from the surface upward, these are as follows:

- Aerosol particles persist through the period in a surface layer that is capped generally beginning at 309 K, oscillating between a well-mixed, isothermal/adiabatic convective layer and relatively distinct nighttime stable layer with relatively high extinction. On 25 September, the convective layer is nearly 2.0 km

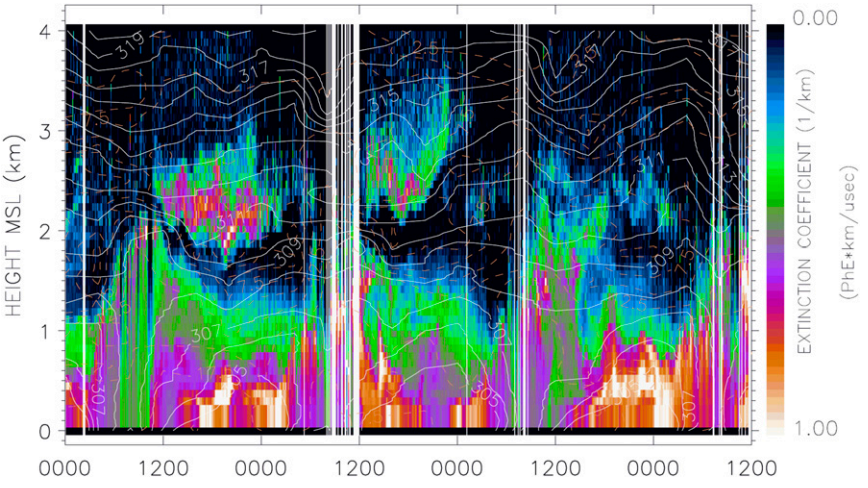

FIG. 7. ALS-derived 355-nm extinction coefficient from 0 to 4 km MSL, with virtual potential temperature isotherms (white solid; K) and water vapor mixing ratio contours (orange dashed; g kg^{-1}) superimposed from collocated 4-hourly radiosonde profiling from 0000 UTC 25 Sep to 1200 UTC 28 Sep 2013 at the Kuching MMD site.

deep, though it does not develop as strongly on the three succeeding days. The nighttime near-surface layer cools to near 304 K on 25 and 26 September, though it is not as cool on the two successive evenings (~305 K). Enhanced nighttime extinction is likely a result both of isentropic particle aggregation and swelling of effective particle size due to cooling and deliquescence (e.g., Cheng et al. 2008).

- The 309-K isotherm was profiled consistently during 25–28 September as the initial cap atop the afternoon convective mixed layer. Beginning 0800 UTC 25 September, a 2–3-K inversion layer (309–311 K) roughly 400 m deep was centered at 2.0 km MSL, with the aerosol extinction coefficient nearly consistent from the surface up through this level. On 26 September, the convective layer did not develop as strongly. Though cloud contamination renders these data somewhat difficult to interpret, the aerosol extinction coefficient exhibits varying gradients with height, capped near about 1.6 km MSL. Light precipitation was observed this afternoon at the site. On 27 September, though not as strong as on 25 September, a distinct mixed convective layer reemerged, though a relatively diffuse thermal cap beginning at 309 K developed above 1.5 km MSL. Extinction coefficients gradients exist within the column, with higher values nearer the surface. A similar structure was observed on 28 September.
- Elevated aerosol particle layers, above 2.0 km MSL, are observed almost exclusively during evening hours on each day, appearing around 1200 UTC. On 25 and 26 September, these layers are decoupled from the surface layer, marked by a distinction in aerosol extinction coefficient that corresponds with the 309–311-K layer capping the surface layer. On 27 September, and corresponding with a relatively weaker thermal cap, the elevated layer appears to be an extension of the surface layer. Given these conflicting scenarios, and considering that back trajectories ending at 2500 m MSL at Kuching did not directly intersect pronounced fire activity along the Borneo coast, and in fact indicate some potential for advection from as far as Sumatra, the source of these aerosols is unclear. In the absence of lower free-tropospheric injection at the source and subsequent downwind advection, however, and considering the proximity of Kuching to the South China Sea, with sea-breeze influence that will be described further below, it is possible that deeper formation of the convective mixed layer is occurring upwind farther inland. That is, with greater surface insolation, it is possible that some areas are experiencing mixing to the surface along the 311-K isotherm, which would allow for convective pumping (Yin et al. 2005) to occur for smoke mass into the free troposphere.
- On 25 and 26 September, each elevated aerosol particle layer corresponds with relatively warm and dry air. This is not so clear on 27 September, though relative local minima in VPT and water vapor mixing ratio are distinct. Two conflicting interpretations of these features are possible. Do they reflect particle swelling and vapor uptake (e.g., Reid et al. 2005) combined with semidirect heating of the surrounding air mass (e.g., Johnson et al. 2004)? If so, does the relative significance of the thermodynamic gradients observed, and compared with those on 27 September, indicate semidirect influence on the layer over time and thus transport? Or does such relatively warm and

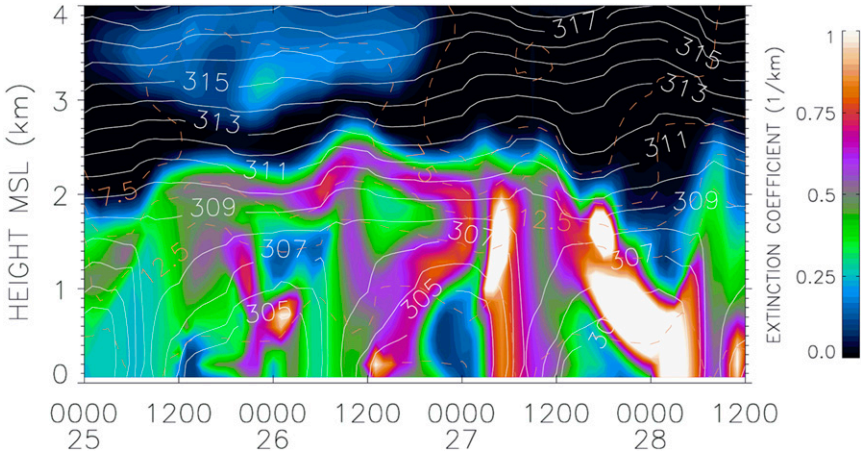

FIG. 8. WRF-Chem simulations of the 355-nm extinction coefficient from 0 to 4 km MSL, resolved at hourly resolution, with corresponding virtual potential temperature isotherms (white solid; K) and water vapor mixing ratio contours (orange dashed; g kg^{-1}) superimposed from 0000 UTC 25 Sep to 1200 UTC 28 Sep 2013 at the 9-km^2 grid cell corresponding to the Kuching MMD site.

dry air represent the only practical condition sustaining their persistence, given that a cooler and moister environment would likely favor cloud formation and, thus, aerosol uptake and potential removal? It is likely that both factors are contributing simultaneously.

4. Characterizing differences between observations and WRF-Chem

a. *Model output*

Based on the configuration chosen for WRF-Chem for this study, simulation output for the 84-h period is shown beginning with Fig. 8, which is a reproduction of Fig. 7 from the model perspective that includes the 355-nm aerosol particle extinction coefficient, VPT, and water vapor mixing ratio. Corresponding with Fig. 8, shown in Fig. 9a are total model aerosol particle mass concentration (μg m^{-3}), and respective contributions from what prove to be lesser aerosol species within the system: soils (Fig. 9b), sea salts (Fig. 9c), and sulfates (Fig. 9d). Differences between Fig. 9a and Figs. 9b–d thus reflect the overwhelming contribution of smoke to the total model mass field.

In Fig. 10, MPLNET- and model-estimated 355-nm AODs are reported at hourly resolution through the period and compared with fine-mode 500-nm level 2.0 AERONET data where spectral decomposition inversion algorithms were successful. WRF-Chem extinction coefficient and column-integrated AOD were calculated native within the model at 600 nm and converted to 355 nm using an Ångstrom exponent of 1.5, an approximation based on previous studies of smoke (e.g., Reid et al. 1999) applied so as to retain an hourly estimate from the model rather than an intermittent one derived using the few available level 2 Ångstrom exponent values derived by AERONET during this period (note also that the 600-nm model AOD was used in lieu of a 355-nm approximation based on either the 300- or 400-nm model solutions to make the comparison with AERONET 500-nm AOD more direct). However, also shown in Fig. 10 are estimates of 355-nm fine-mode AOD approximated using an offline version of the O'Neill et al. (2003) spectral decomposition algorithm. Spectral Ångstrom exponents solved from these data ranged between 1.10 and 1.50, suggesting that the 355-nm model AOD estimates are likely high-end approximations. Further, comparison of MPLNET AOD with these fine-mode 500-nm level 2.0 AERONET data indicates that 60 sr was often a low-end approximation for the lidar ratio.

Shown in Fig. 11 are surface mass concentrations for particles of diameter less than 2.5 μm, with corresponding surface winds superimposed, every 12 h from 0000 UTC 25 September to 1200 UTC 28 September, which depicts the evolution of smoke originating along the western Borneo coastline through the simulation. Furthermore, these data indicate that model trajectories were indeed consistent with those estimated using HYSPLIT analysis above and thus that the model was indeed resolving smoke at Kuching based predominantly on advection from fires originating along the western coastline. This point is reinforced by comparison of radiosonde and model wind profiles (Fig. 12), which is explored further below.

b. *Primary model differences with observations*

Considering the likely low-end MPLNET-based solutions for extinction, and thus AOD, compared with

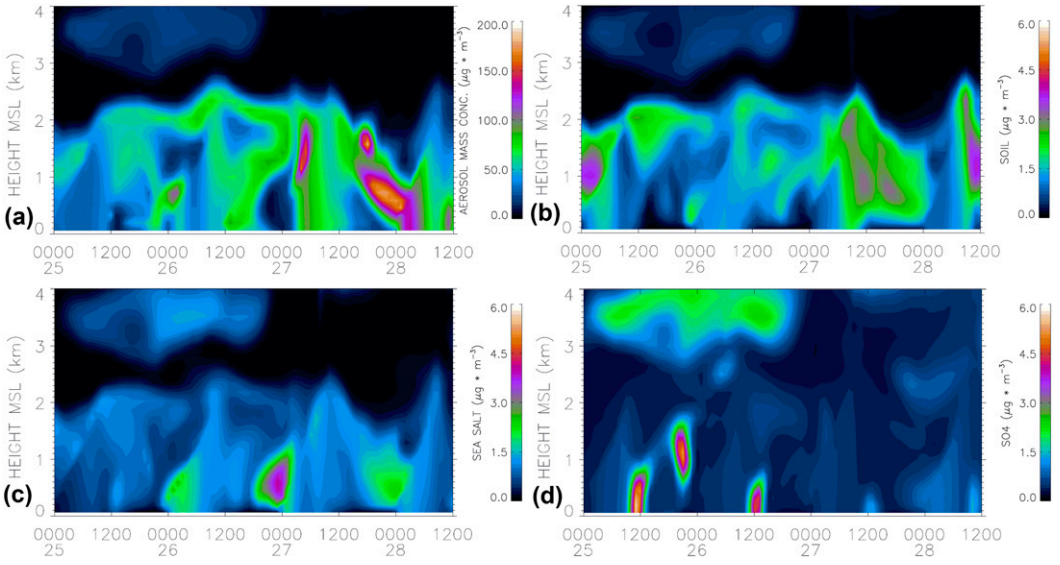

FIG. 9. Corresponding to the WRF-Chem simulations in Fig. 7, (a) total aerosol mass concentration ($\mu g\,m^{-3}$) and speciated total concentrations for (b) soils, (c) sea salt, and (d) sulfates (SO_4).

corresponding high-end approximations from the model, the latter result is very likely underestimating AOD. Though we do not specifically identify the impact and potential bias of prescribed model microphysics on this result, we conclude that, by proxy, the model is low with respect to total mass concentration. One exception occurs early on 27 September, corresponding with a relatively dense, albeit brief, layer of high extinction near 1–2 km. The model further resolves AOD maxima on 27 and 28 September that match well with the lidar. However, the corresponding layers are relatively well concentrated vertically, suggesting nearby smoke plume advection within the modeling domain that does not necessarily verify well with observation. Further, though the model resolves aerosol mass to depths of 2.0–2.5 km MSL overall, there is no apparent delineation of elevated layers, save for a diffuse layer above 3.0 km persisting on 25 and 26 September, which shows a diurnal pattern different from those elevated features resolved in the in situ data.

Shown in Fig. 13a are differences in the 355-nm aerosol particle extinction coefficient between MPLNET ALS and WRF-Chem. Three distinct features of the model analysis differ noticeably from observation. First, the model fails to resolve the diurnal oscillation of enhanced particle extinction within the nighttime stable surface layer. Second, aside from maxima resolved on 27 and 28 September, the model resolves its most significant smoke within the thermal cap layer atop the mixed layer (309–311 K), which does not appear either decoupled from the surface layer or mixed sufficiently into the free troposphere. In contrast, ALS observations show that this depth is mostly free of significant particle scattering. Instead, and third, ALS observations indicate that particle mixing is occurring above this level into the free troposphere that, again, the model does not resolve. In total, the model depicts more particle extinction relative to ALS at the top of the mixed layer and is lower nearer the surface.

It is first reasonable to skeptically question whether or not the model meteorological fields verify with any skill and thus whether or not the simulations were compromised by deficient core thermodynamics. We begin this analysis by noting that the FNL global model used to

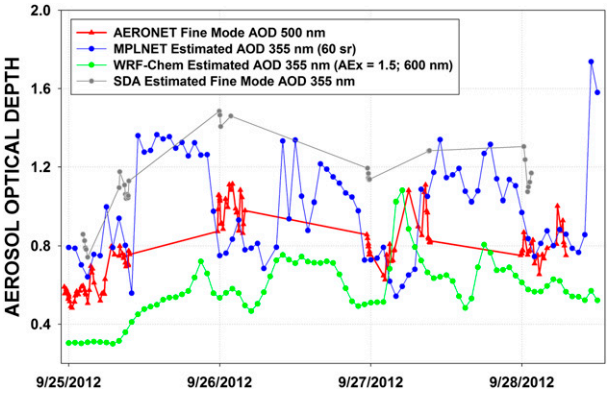

FIG. 10. Level 2.0 AERONET fine-mode 500-nm AOD (red); MPLNET ALS-estimated 355-nm AOD (blue), using an extinction-to-backscatter ratio of 60 sr; WRF-Chem-estimated 355-nm AOD (green), derived from 600-nm model output using an Ångstrom exponent of 1.5; and an offline 355-nm estimate based on spectral decomposition of AERONET AOD (gray) from 0000 UTC 25 Sep to 1200 UTC 28 Sep 2013.

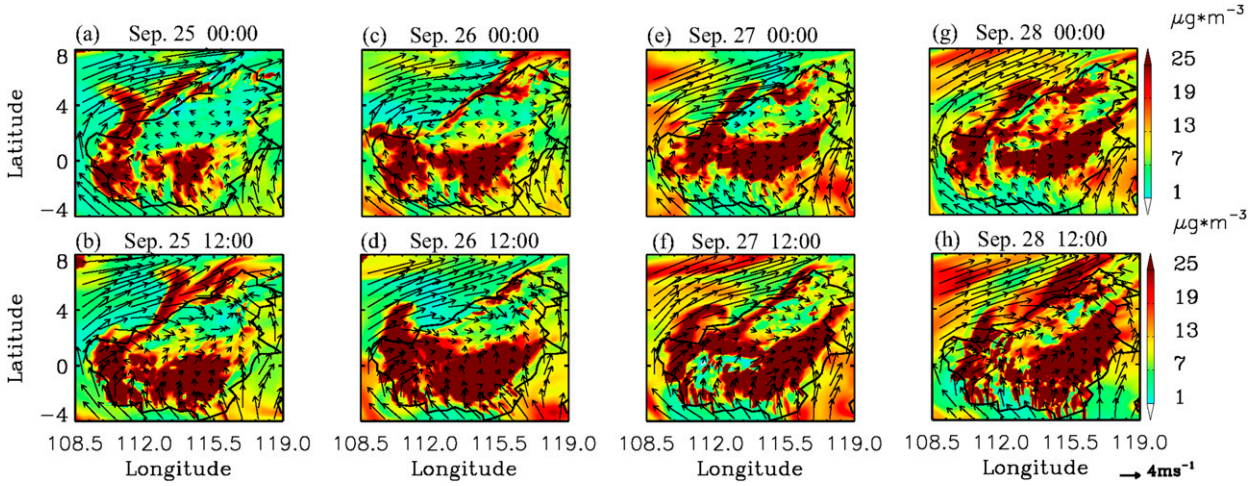

FIG. 11. Corresponding to WRF-Chem simulations in Fig. 7, surface-based aerosol particle mass concentrations (g μg^{-1}) for diameters less than 2.5 μm centered around Borneo at (a) 0000 and (b) 1200 UTC 25 Sep, (c) 0000 and (d) 1200 UTC 26 Sep, (e) 0000 and (f) 1200 UTC 27 Sep, and (g) 0000 and (h) 1200 UTC 29 Sep. Model surface wind speeds are superimposed, with magnitude (m s^{-1}) scaled according to the sample barb shown with (h).

supply boundary conditions for the WRF-Chem simulation includes assimilation of the WMO-based radiosonde profiles collected on site at 0000 and 1200 UTC. Therefore, the model is receiving regular updates for conditions directly at Kuching, corresponding roughly with local sunrise and sunset hours.

Figures 12a and 12b feature radiosonde (25 m) and model (100 m) winds (see legend for definition of wind barbs). Differences between these two plots, at 100-m vertical resolution, are shown in Fig. 13d (note the missing radiosonde profile at 0600 UTC 26 September). The proximity of Kuching to the South China Sea results in a significant land/sea-breeze component, which is evident in Fig. 12a below 1.5 km MSL. In general, model wind errors rarely exceed 5 m s^{-1} (maxima in some instances do approach 10 m s^{-1}) and then only at the top of the mixed layer. Nearer the surface, model wind errors are lower, and in many instances insignificant. This performance is consistent with the results of Wang et al. (2013), who identify similarly reasonable skill exhibited by WRF-Chem in resolving land/sea-breeze phenomena on Borneo.

Differences in VPT and water vapor mixing ratio solved between observations and WRF-Chem are next shown in Figs. 13b and 13c, respectively. Some isentropic offsets are apparent, though their magnitudes are relatively small (~1–2 K) and confined to the near-surface and top of the convective mixed layer. Observations are almost exclusively warmer than the model. Lack of vertical development of the mixed layer on 25 and 26 September persists as 1–2-K model cold biases between 1.5 and 2.5 km through the nighttime hours each day. Static stability atop the mixed layer is too strong in the model on 28 September, as convective mixing was occurring above that height into the lower free troposphere. In general, however, and combined with winds, model thermodynamics to this point are reasonable.

Some large differences do exist in water vapor mixing ratio fields, with the model reaching a maximum 6 g kg^{-1} too high near 2 km at 1600 UTC 26 September. Notably, the three largest model overestimates of this parameter, between 1 and 2 km after 0000 UTC 25 September, the same depths near 0000 UTC 26 September, and closer to 2 km after 1200 UTC 26 September, each correspond with areas where the model overestimates aerosol particle extinction. Smoke particle presence and advection sufficiently downwind of active fires in SEA/MC conceptually corresponds with relatively dry air masses, less the increased potential for cloud nucleation, uptake, and wet deposition that would inhibit sustained downwind propagation. Though this aspect of the analysis requires further study, this result does not necessarily impact our otherwise favorable impression toward the fidelity of the model meteorological fields. Otherwise, model water vapor underestimates are generally less than 4 g kg^{-1}.

c. *Distinguishing primary causes of model differences*

Leaving aside differences in modeled water vapor mixing ratios near the top of the surface mixed layer, the primary differences between WRF-Chem output and observation involve total model aerosol mass and the vertical profile for the particle extinction coefficient. Though a confluence of processes, including core dynamic

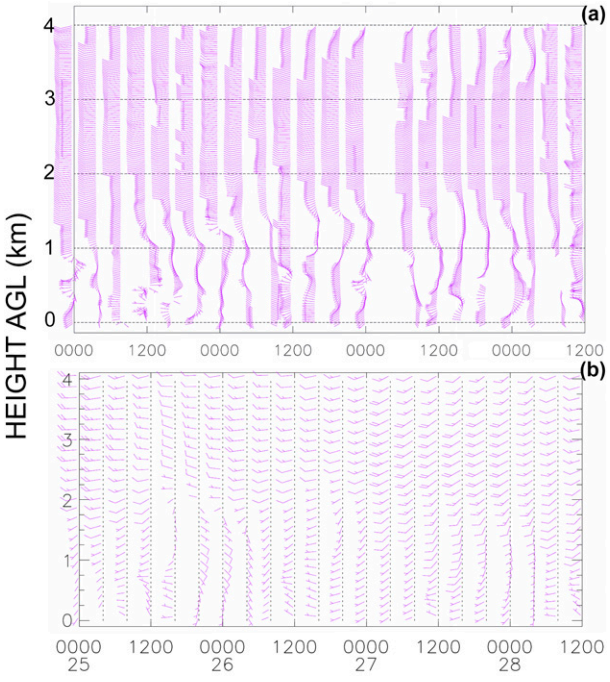

FIG. 12. Wind vectors (speed; m s^{-1}) solved at (a) 25-m vertical resolution for 0–4 km MSL from 4-hourly radiosonde launches conducted at the Kuching MMD site (the 0400 UTC 27 Sep profile was removed because of poor data) and (b) WRF-Chem simulations at 4-hourly resolution for the 11 terrain-following hydrostatic pressure coordinate levels found between the ground and 4 km MSL from 0000 UTC 25 Sep to 1200 UTC 28 Sep 2013. Null barbs are <1 m s^{-1}; dashed staffs are 1–5 m s^{-1}; half barbs are 5–9 m s^{-1}; full barbs are 10–14 m s^{-1}; and full + half barbs are 15 m s^{-1} and higher.

and radiative parameterization schemes, surely contributes to the overall result, the most significant differences are believed to be the result of the following:

- FLAMBE regional smoke source emission inventories being low overall.
- The static parameterization of a single smoke injection height is likely misrepresentative, which impacts how particle mixing occurs within the model column, and in particular within the diurnally evolving convective boundary layer, during transport downwind.

Furthermore, the diurnal decoupling of elevated smoke above the convective boundary layer and enhancement in nighttime near-surface extinction from likely hygroscopic effects, both prominent in the in situ data, are absent from the simulations. Further investigation is necessary to identify which components of the model are responsible for their reconciliation.

Smoke emission inventories regardless of methodology, though particularly in the MC, suffer globally from significant errors of omission. The most important of these is the large fraction of fires that are too small to be reliably detected with the current generation of space-based instruments (Schroeder et al. 2008; Miettinen and Liew 2009). This problem is exacerbated by the frequency of low-level liquid water cloud presence that inhibits surface 4-μm monitoring used in level 2 MODIS fire detection products (Holz et al. 2008; Miettinen et al. 2013). Though the two-day maximum fire correction applied to FLAMBE was designed to limit these effects, this relates only to fires captured by MODIS and does not fully compensate for those never detected in the first place. Model experiments can provide climatological scaling factors (e.g., Reid et al. 2009). However, as errors of omission will not be constant across the region and across seasons (Reid et al. 2012), regional scaling will not necessarily improve the representation of emissions patterns at relatively fine scales.

Use of the static 800-m smoke injection height parameterization is based on model tuning to seasonal CALIOP-based regional aerosol profiles (Wang et al. 2013). Colarco et al. (2004) consider the sensitivity of the smoke injection scenario and its impact on model skill. They further describe historical efforts to refine this parameterization and the significance of convective and synoptic-scale dynamic processes at the source and along transport trajectories that determine how representative the smoke profile looks versus observation downwind. Taken together with Wang et al. (2010, 2013), for a given climate regime and emissions of a certain scale and convective/mixing potential, an effective model injection scenario (even one as simple as a static 800 m) can be derived through tuning that produces reasonably stable results over time. One factor not considered or previously tested, however, is the time necessary for the model, for any given input profile, to diffuse advecting particle mass vertically so as to achieve such proficiency. In this study, and considering what is only roughly 1–2 days from source to observation (Fig. 6), the static assumption of 800-m injection is potentially coarse.

Aside from model source emissions, the lack of elevated smoke aerosol particle presence above the surface layer each afternoon is conspicuous, as is the lack of diurnal variance in extinction within the cooling near-surface layer. Evidence collected by MPLNET for fires burning in southern Borneo indicate that aerosol particle mass does not reach the free troposphere at the source (not shown). Buoyancy and the potential for lifting mass above thermal inversions nearest the surface depend on fire radiative power and effective size, which varies from fire to fire regionally (e.g., Peterson et al. 2015). In Southeast Asia, fire size is limited by the moist ambient environment. Campbell et al. (2013) conclude

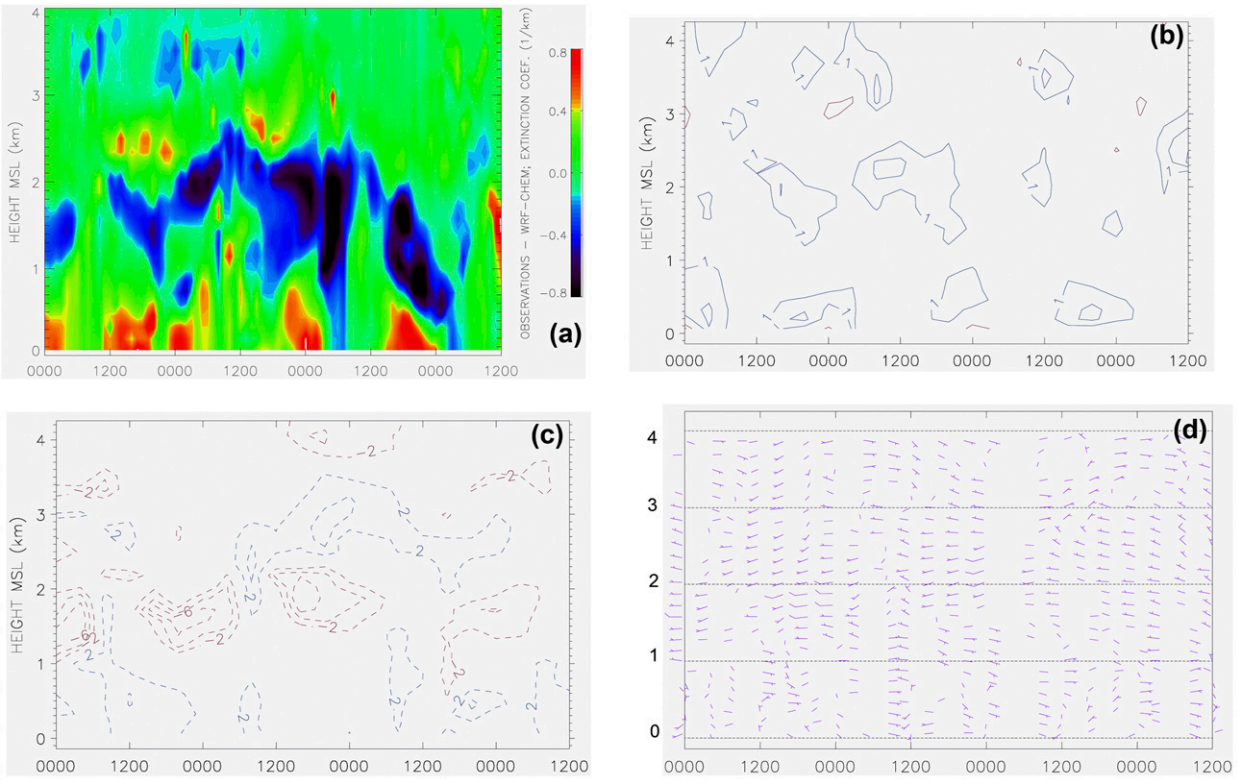

FIG. 13. From Figs. 7, 8, and 12, at the Kuching MMD site from 0000 UTC 25 Sep to 1200 UTC 28 Sep: (a) differences between the Kuching ALS and WRF-Chem solutions for the 355-nm extinction coefficient at hourly resolution, and differences between Kuching radiosonde profiling and WRF-Chem solutions at 4-hourly resolution (blue are positive and red are negative relative differences) for (b) virtual potential temperature (K), (c) water vapor mixing ratio ($g\,kg^{-1}$), and (d) interpolated (see text) wind vectors ($m\,s^{-1}$).

that little particle mass reaches and/or settles into the lower free troposphere regionally. Therefore, if smoke particles are not readily reaching the lower free troposphere at their source, convective mixing during the warm afternoon is the only other plausible mechanism for inducing free-tropospheric displacement. Evidence for this is apparent on 27 September, for instance.

5. Conclusions

An experiment conducted by the Naval Research Laboratory and the NASA Micro-Pulse Lidar Network (MPLNET) and Aerosol Robotic Network (AERONET) projects is described, having collected continuous ground-based lidar, sun photometer, and 4-h radiosonde thermodynamic profiling over 84 consecutive hours during an anthropogenic biomass burning event at Kuching, Malaysia, on northwestern Borneo in the southern Maritime Continent of Southeast Asia. Although local fires near Kuching were active, the primary source of the smoke observed was situated roughly 300–500 km (~1–2 days) upwind of the site along the western Borneo coast. The period was distinct for the lack of any significant precipitation observed, providing near-ideal conditions for observing advecting smoke at this near-coastal tropical site. However, satellite observation during the period and surface sun photometry were compromised by persistent cirrus cloud coverage overhead, leaving the synergistic lidar/radiosonde profiling as the primary observations collected.

With these data, smoke transport simulations are evaluated for skill at Kuching using a well-characterized mesoscale version of the WRF-Chem model. Model depictions of smoke distribution and its optical properties are compared with the lidar/sun photometer, and thermodynamic parameters, including winds, are compared with the relatively high-resolution radiosonde data. Overall, the simulations are reasonable. Important differences between the model and observations are found, however. First-order model processes are identified as the most likely explanations for these differences. Sensitivity analysis of model parameterizations is not undertaken in this initial study. Model depictions of total aerosol particle extinction, and thus by proxy mass concentration, are low relative to observation. This is attributable to underestimates for regional smoke

emissions over Borneo, because of both the infrequent and suboptimal schedule of observations by sun-synchronous satellites as well as inhibition by opaque clouds of the MODIS 4-μm signal from fires that drives the model source Fire Locating and Modeling of Burning Emissions (FLAMBE) product.

The vertical profile for modeled aerosol particle extinction exhibits distinct differences with observation. This is found in spite of model thermodynamic analyses that exhibit reasonable skill when compared with 4-h radiosonde profiling. Offsets in virtual potential temperature (VPT), water vapor mixing ratios, and wind vectors are relatively small in most instances, though this is not a fully independent comparison, owing to the 6-hourly updates to the WRF-Chem boundary conditions from FNL meteorological reanalyses. The Kuching site is a regular WMO radiosonde site, and thus 0000 and 1200 UTC radiosonde information is directly assimilated within the model analysis. The use of a static smoke source injection height, tuned to match seasonal satellite-based climatological profiles, potentially compromises overall skill. It is proposed that the time necessary for the model to equilibrate and mix smoke uniformly exceeds that between emissions and advection downwind to Kuching in this case.

The model does not resolve elevated smoke particle layers observed diurnally within the lower free troposphere. As significant smoke particle mass is not believed to reach this level at the source, mixing is likely occurring during transport downwind through afternoon convective processes, the cyclical structure of which the model is not resolving. Further, significant differences are found in extinction values nearest the surface, corresponding with nighttime cooling and likely hygroscopic particle growth. These processes each require subsequent study and reconciliation.

This case study reflects a relatively simple aerosol transport event: a single aerosol source, experiencing relatively little downwind mixing, transported mostly over land for 1–2 days and 300–500 km. Important differences between the model and observations indicate areas where improvements to model inputs and physical processes can be improved. Ultimately, though, there will always be limitations to what models are capable of resolving, with respect to spatial and temporal scales of aerosol particle mass advection. As the skill and efficacy of atmospheric models improve, however, novel sources of validation data will be necessary, and limitations of satellite-based datasets, especially in regions with persistent cloud cover, may dictate that detailed in situ observations of the type used in this study are necessary for models to make tangible improvements. Utilization of these novel datasets is not always straightforward, however, and active collaboration between observation and modeling communities will be imperative to obtaining the best return on investment in both model development and observational datasets.

Acknowledgments. Deployment of the Micro-Pulse Lidar Network (MPLNET) ALS, Aerosol Robotic Network (AERONET) sun photometer, and Naval Research Laboratory (NRL) radiation instrument package to Kuching during summer 2012 could not have been achieved without the critical support and collaboration of the Malaysian Meteorological Department (MMD), National University of Malaysia, and National University of Singapore. Special thanks are given to our MMD colleagues in Kuching, including State Director of Sarawak MMD Wong Teck Kiong, Kuching Meteorological Observation Station Manager Tan Kok Chong, and Kuching Radiosonde Coordinator Justin Lim Swee Hian. Further, to the staff at the Kuching MMD station, we owe our collective gratitude for kindly hosting us and assisting our supplemental radiosonde launches. Our humble appreciation for the assistance, encouragement, and patience of all of these groups and individuals cannot be overstated. Sebastian Schmidt and Phillip Haftings (MPLNET) and Gautier Veroone and Jerome Southammakosane (Leosphere) were indispensable, assisting with instrument operations in the field. NRL and Computer Sciences Corporation participants have received financial support from the Chief of Naval Research through the NRL Base Program (PE 0601153N) and Office of Naval Research Codes 32 (PE 0602435N) and 35 (PE 0602114N). Author Campbell acknowledges the support of NASA Interagency Agreement NNG13HH10I on behalf of MPLNET and the Southeast Asia Composition, Cloud, Climate Coupling Regional Study (SEAC^{4}RS) Science Team (H. Maring). Financial support for MPLNET and AERONET activities comes from the NASA Radiation Sciences Program and SEAC^{4}RS Science Team. Participation by Drs. Wang and Ge for WRF modeling was supported, in part, by the NASA Interdisciplinary Science Program.

REFERENCES

Ackermann, I. J., H. Hass, M. Memmesheimer, A. Ebel, F. S. Binkowski, and U. Shankar, 1998: Modal aerosol dynamics model for Europe: Development and first applications. *Atmos. Environ.*, **32**, 2981–2999, doi:10.1016/S1352-2310(98)00006-5.

Anderson, T. L., R. J. Charlson, D. M. Winker, J. A. Ogren, and K. Holmen, 2003: Mesoscale variations of tropospheric aerosols. *J. Atmos. Sci.*, **60**, 119–136, doi:10.1175/1520-0469(2003)060<0119:MVOTA>2.0.CO;2.

——, and Coauthors, 2005: An "A-Train" strategy for quantifying direct climate forcing by anthropogenic aerosols. *Bull. Amer. Meteor. Soc.*, **86**, 1795–1809, doi:10.1175/BAMS-86-12-1795.

Ansmann, A., H. Baars, M. Tesche, D. Müller, D. Althausen, R. Engelmann, T. Pauliquevis, and P. Artaxo, 2009: Dust and smoke transport from Africa to South America: Lidar profiling over Cape Verde and the Amazon rainforest. *Geophys. Res. Lett.*, **36**, L11802, doi:10.1029/2009GL037923.

Balis, D. S., and Coauthors, 2003: Raman lidar and sunphotometric measurements of aerosol optical properties over Thessaloniki, Greece during a biomass burning episode. *Atmos. Environ.*, **37**, 4529–4538, doi:10.1016/S1352-2310(03)00581-8.

Banta, R. M., and Coauthors, 2005: A bad air day in Houston. *Bull. Amer. Meteor. Soc.*, **86**, 657–669, doi:10.1175/BAMS-86-5-657.

Benedetti, A., and Coauthors, 2009: Aerosol analysis and forecast in the European Centre for Medium-Range Weather Forecasts Integrated Forecast System: 2. Data assimilation. *J. Geophys. Res.*, **114**, D13205, doi:10.1029/2008JD011115.

Campbell, J. R., and Coauthors, 2013: Characterizing the vertical profile of aerosol particle extinction and linear depolarization over Southeast Asia and the Maritime Continent: The 2007–2009 view from CALIOP. *Atmos. Res.*, **122**, 520–543, doi:10.1016/j.atmosres.2012.05.007.

Chapman, E. G., W. I. Gustafson Jr., R. C. Easter, J. C. Barnard, S. J. Ghan, M. S. Pekour, and J. D. Fast, 2009: Coupling aerosol–cloud–radiative processes in the WRF-Chem model: Investigating the radiative impact of elevated point sources. *Atmos. Chem. Phys.*, **9**, 945–964, doi:10.5194/acp-9-945-2009.

Cheng, Y. F., and Coauthors, 2008: Relative humidity dependence of aerosol optical properties and direct radiative forcing in the surface boundary layer at Xinken in Pearl River Delta of China: An observation based numerical study. *Atmos. Environ.*, **42**, 6373–6397, doi:10.1016/j.atmosenv.2008.04.009.

Chew, B. N., J. R. Campbell, J. S. Reid, E. J. Welton, S. V. Salinas, and S. C. Liew, 2013: Aerosol particle properties and their vertical distribution over Singapore. *Atmos. Environ.*, **79**, 599–613, doi:10.1016/j.atmosenv.2013.06.026.

Chin, M., and Coauthors, 2002: Tropospheric aerosol optical thickness from the GOCART model and comparisons with satellite and sun photometer measurements. *J. Atmos. Sci.*, **59**, 461–483, doi:10.1175/1520-0469(2002)059<0461:TAOTFT>2.0.CO;2.

Colarco, P. R., M. R. Schoeberl, B. G. Doddridge, L. T. Marufu, O. Torres, and E. J. Welton, 2004: Transport of smoke from Canadian forest fires to the surface near Washington, D.C.: Injection height, entrainment, and optical properties. *J. Geophys. Res.*, **109**, D06203, doi:10.1029/2003JD004248.

——, A. da Silva, M. Chin, and T. Diehl, 2010: Online simulations of global aerosol distributions in the NASA GEOS-4 model and comparisons to satellite and ground-based aerosol optical depth. *J. Geophys. Res.*, **115**, D14207, doi:10.1029/2009JD012820.

——, R. A. Khan, L. A. Remer, and R. C. Levy, 2014: Impact of satellite viewing-swath width on global and regional aerosol optical thickness statistics and trends. *Atmos. Meas. Tech.*, **7**, 2313–2335, doi:10.5194/amt-7-2313-2014.

Draxler, R. R., and G. D. Rolph, 2013: HYSPLIT—Hybrid Single Particle Lagrangian Integrated Trajectory Model. NOAA Air Resource Laboratory, accessed 1 June 2013. [Available online at http://www.arl.noaa.gov/HYSPLIT.php.]

Fernald, F. G., 1984: Analysis of atmospheric lidar observations: Some comments. *Appl. Opt.*, **23**, 652–653, doi:10.1364/AO.23.000652.

Fuller, D. O., and K. Murphy, 2006: The ENSO–fire dynamic in insular Southeast Asia. *Climatic Change*, **74**, 435–455, doi:10.1007/s10584-006-0432-5.

Ge, C., J. Wang, and J. S. Reid, 2014: Mesoscale modeling of smoke transport over the Southeast Asian Maritime Continent: Coupling of smoke direct radiative feedback below and above low-level clouds. *Atmos. Chem. Phys.*, **14**, 159–174, doi:10.5194/acp-14-159-2014.

Gettelman, A., and P. M. de F. Forster, 2002: A climatology of the tropical tropopause layer. *J. Meteor. Soc. Japan*, **80**, 911–924, doi:10.2151/jmsj.80.911.

——, ——, M. Fujiwara, Q. Fu, H. Vomel, L. K. Gohar, C. Johanson, and M. Ammerman, 2004: Radiation balance of the tropical tropopause layer. *J. Geophys. Res.*, **109**, D07103, doi:10.1029/2003JD004190.

Ghan, S. J., and S. E. Schwartz, 2007: Aerosol properties and processes: A path from field and laboratory measurements to global climate models. *Bull. Amer. Meteor. Soc.*, **88**, 1059–1083, doi:10.1175/BAMS-88-7-1059.

Grell, G. A., and D. Devenyi, 2002: A generalized approach to parameterizing convection combining ensemble and data assimilation techniques. *Geophys. Res. Lett.*, **29**, 38-1–38-4, doi:10.1029/2002GL015311.

——, S. E. Peckham, R. Schmitz, S. A. McKeen, G. Frost, W. C. Skamarock, and B. Eder, 2005: Fully coupled "online" chemistry within the WRF model. *Atmos. Environ.*, **39**, 6957–6975, doi:10.1016/j.atmosenv.2005.04.027.

Guenther, A., P. Zimmerman, and M. Wildermuth, 1994: Natural volatile organic compound emission rate estimates for U.S. woodland landscapes. *Atmos. Environ.*, **28**, 1197–1210, doi:10.1016/1352-2310(94)90297-6.

Holben, B. N., and Coauthors, 1998: AERONET—A federated instrument network and data archive for aerosol characterization. *Remote Sens. Environ.*, **66**, 1–16, doi:10.1016/S0034-4257(98)00031-5.

Hollingsworth, A., R. J. Engelen, A. Benedetti, A. Dethof, J. Felmming, J. W. Kaiser, J.-J. Morcrette, and A. J. Simmons, 2008: Toward a monitoring and forecasting system for atmospheric composition: The GEMS project. *Bull. Amer. Meteor. Soc.*, **89**, 1147–1164, doi:10.1175/2008BAMS2355.1.

Holz, R. E., S. A. Ackerman, F. W. Nagle, R. Frey, S. Dutcher, R. E. Kuehn, M. A. Vaughan, and B. Baum, 2008: Global Moderate Resolution Imaging Spectroradiometer (MODIS) cloud detection and height evaluation using CALIOP. *J. Geophys. Res.*, **113**, D00A19, doi:10.1029/2008JD009837.

Hong, S.-Y., Y. Noh, and J. Dudhia, 2006: A new vertical diffusion package with an explicit treatment of entrainment processes. *Mon. Wea. Rev.*, **134**, 2318–2341, doi:10.1175/MWR3199.1.

Hyer, E. J., and B. N. Chew, 2010: Aerosol transport model evaluation of an extreme smoke episode in Southeast Asia. *Atmos. Environ.*, **44**, 1422–1427, doi:10.1016/j.atmosenv.2010.01.043.

——, J. S. Reid, and J. Zhang, 2011: An over-land aerosol optical depth data set for data assimilation by filtering, correction, and aggregation of MODIS Collection 5 optical depth retrievals. *Atmos. Meas. Tech.*, **4**, 379–408, doi:10.5194/amt-4-379-2011.

——, ——, E. M. Prins, J. P. Hoffman, C. C. Schmidt, J. I. Miettinen, and L. Giglio, 2013: Patterns of fire activity over

Indonesia and Malaysia from polar and geostationary satellite observations. *Atmos. Res.*, **122**, 504–519, doi:10.1016/j.atmosres.2012.06.011.

Jensen, E. J., A. S. Ackerman, and J. A. Smith, 2007: Can overshooting convection dehydrate the tropical tropopause layer? *J. Geophys. Res.*, **112**, D11209, doi:10.1029/2006JD007943.

Johnson, B. T., K. P. Shine, and P. M. Forster, 2004: The semidirect aerosol effect: Impact of absorbing aerosol on marine stratocumulus. *Quart. J. Roy. Meteor. Soc.*, **130**, 1407–1422, doi:10.1256/qj.03.61.

King, M. D., and Coauthors, 2003: Cloud and aerosol properties, precipitable water and profiles of temperature and water vapor from MODIS. *IEEE Trans. Geosci. Remote Sens.*, **41**, 442–458, doi:10.1109/TGRS.2002.808226.

Kinne, S., and Coauthors, 2005: An AeroCom initial assessment—Optical properties in aerosol component modules of global models. *Atmos. Chem. Phys.*, **5**, 8285–8330, doi:10.5194/acpd-5-8285-2005.

Koffi, B., and Coauthors, 2012: Application of the CALIOP layer product to evaluate the vertical distribution of aerosols estimated by global models: AeroCom phase I results. *J. Geophys. Res.*, **117**, D10201, doi:10.1029/2011JD016858.

Langmann, B., A. Folch, M. Hensch, and V. Matthias, 2012: Volcanic ash over Europe during the eruption of Eyjafjallajökull on Iceland, April–May 2010. *Atmos. Environ.*, **48**, 1–8, doi:10.1016/j.atmosenv.2011.03.054.

Langner, A. J., F. Miettinen, and F. Siegert, 2007: Land cover change 2002–2005 in Borneo and the role of fire derived from MODIS imagery. *Global Change Biol.*, **13**, 2329–2340, doi:10.1111/j.1365-2486.2007.01442.x.

Li, A., and Coauthors, 2009: Uncertainties in satellite remote sensing of aerosols and impact on monitoring its long-term trend: A review and perspective. *Ann. Geophys.*, **27**, 2755–2770, doi:10.5194/angeo-27-2755-2009.

Lin, Y.-L., R. D. Farley, and H. D. Orville, 1983: Bulk parameterization of the snow field in a cloud model. *J. Climate Appl. Meteor.*, **22**, 1065–1092, doi:10.1175/1520-0450(1983)022<1065:BPOTSF>2.0.CO;2.

Liu, Y., and Coauthors, 2008: The operational mesogamma-scale analysis and forecast system of the U.S. Army Test and Evaluation Command. Part 1: Overview of the modeling system, the forecast products. *J. Appl. Meteor. Climatol.*, **47**, 1077–1092, doi:10.1175/2007JAMC1653.1.

Lohmann, U., J. Quaas, S. Kinne, and J. Feichter, 2007: Different approaches for constraining global climate models of the anthropogenic indirect aerosol effect. *Bull. Amer. Meteor. Soc.*, **88**, 243–249, doi:10.1175/BAMS-88-2-243.

Lolli, S., L. Sauvage, S. Loaec, and M. Lardier, 2011: EZ Lidar: A new compact autonomous eye-safe scanning aerosol lidar for extinction measurements and PBL height detection: Validation of the performances against other instruments and intercomparison campaigns. *Opt. Pura Apl.*, **44**, 33–41.

Magi, B. I., P. Ginoux, Y. Ming, and V. Ramaswamy, 2009: Evaluation of tropical and extratropical Southern Hemisphere African aerosol properties simulated by a climate model. *J. Geophys. Res.*, **114**, D14204, doi:10.1029/2008JD011128.

Mahmud, M., 2009: Mesoscale model simulation of low level equatorial winds over Borneo during the haze episode of September 1997. *J. Earth Syst. Sci.*, **118**, 295–307, doi:10.1007/s12040-009-0032-7.

——, 2013: Assessment of atmospheric impacts of biomass open burning in Kalimantan, Borneo during 2004. *Atmos. Environ.*, **78**, 242–249, doi:10.1016/j.atmosenv.2012.03.019.

McFarquhar, G. M., A. J. Heymsfield, J. Spinhirne, and B. Hart, 2000: Thin and subvisual tropopause tropical cirrus: Observations and radiative impacts. *J. Atmos. Sci.*, **57**, 1841–1853, doi:10.1175/1520-0469(2000)057<1841:TASTTC>2.0.CO;2.

Miettinen, J., and S. C. Liew, 2009: Burn-scar patterns and their effect on regional burnt-area mapping in insular South-east Asia. *Int. J. Wildland Fire*, **18**, 837–847, doi:10.1071/WF08102.

——, and ——, 2010: Degradation and development of peatlands in Peninsular Malaysia and in the islands of Sumatra and Borneo since 1990. *Land Degrad. Dev.*, **21**, 285–296, doi:10.1002/ldr.976.

——, C. Shi, and S. C. Liew, 2011: Influence of peatland and land cover distribution on fire regimes in insular Southeast Asia. *Reg. Environ. Change*, **11**, 191–201, doi:10.1007/s10113-010-0131-7.

——, E. Hyer, A. S. Chia, L. K. Kwoh, and S. C. Liew, 2013: Detection of vegetation fires and burnt areas by remote sensing in insular Southeast Asian conditions: Current status of knowledge and future challenges. *Int. J. Remote Sens.*, **34**, 4344–4366, doi:10.1080/01431161.2013.777489.

Morcrette, J.-J., and Coauthors, 2009: Aerosol analysis and forecast in the European Centre for Medium-Range Weather Forecasts Integrated Forecast System: Forward modeling. *J. Geophys. Res.*, **114**, D06206, doi:10.1029/2008JD011235.

Mu, M., and Coauthors, 2011: Daily and 3-hourly variability in global fire emissions and consequences for atmospheric model predictions of carbon monoxide. *J. Geophys. Res.*, **116**, D24303, doi:10.1029/2011JD016245.

Müller, D., I. Mattis, U. Wandinger, A. Ansmann, D. Althausen, and A. Stohl, 2005: Raman lidar observations of aged Siberian and Canadian forest fire smoke in the free troposphere over Germany in 2003: Microphysical particle characterization. *J. Geophys. Res.*, **110**, D17201, doi:10.1029/2004JD005756.

Noh, Y. M., Y. J. Kim, B. C. Choi, and T. Murayama, 2007: Aerosol lidar ratio characteristics measured by a multi-wavelength Raman lidar system at Anmyeon Island, Korea. *Atmos. Res.*, **86**, 76–87, doi:10.1016/j.atmosres.2007.03.006.

O'Dowd, C., and Coauthors, 2012: The Eyjafjallajökull ash plume—Part II: Forecasting the plume dispersion. *Atmos. Environ.*, **48**, 143–151, doi:10.1016/j.atmosenv.2011.10.037.

O'Neill, N. T., T. F. Eck, A. Smirnov, B. N. Holben, and S. Thulasiraman, 2003: Spectral discrimination of coarse and fine mode optical depth. *J. Geophys. Res.*, **108**, 4559, doi:10.1029/2002JD002975.

Page, S. E., F. Siegert, J. O. Rieley, H.-D. V. Boehm, A. Jaya, S. Limin, 2002: The amount of carbon released from peat and forest fires in Indonesia during 1997. *Nature*, **420**, 61–65, doi:10.1038/nature01131.

Pérez, C., S. Nickovic, G. Pejanovic, J. M. Baldasano, and E. Özsoy, 2006: Interactive dust-radiation modeling: A step to improve weather forecasts. *J. Geophys. Res.*, **111**, D16206, doi:10.1029/2005JD006717.

Peterson, D. A., E. J. Hyer, J. R. Campbell, M. D. Fromm, J. W. Hair, C. F. Butler, and M. A. Fenn, 2015: The 2013 Rim Fire: Implications for predicting extreme fire spread, pyroconvection, and smoke emission. *Bull. Amer. Meteor. Soc.*, **96**, 229–247, doi:10.1175/BAMS-D-14-00060.1.

Reid, J. S., T. F. Eck, S. A. Christopher, P. V. Hobbs, and B. Holben, 1999: Use of the Ångstrom exponent to estimate the variability of optical and physical properties of aging smoke particles in Brazil. *J. Geophys. Res.*, **104**, 27 473–27 489, doi:10.1029/1999JD900833.

——, R. Koppmann, T. Eck, and D. Eleuterio, 2005: A review of biomass burning emissions part II: Intensive physical properties

of biomass burning particles. *Atmos. Chem. Phys.*, **5**, 799–825, doi:10.5194/acp-5-799-2005.

——, and Coauthors, 2009: Global monitoring and forecasting of biomass burning smoke: Description and lessons from the Fire Locating and Modeling of Burning Emissions (FLAMBE) program. *IEEE J. Sel. Top. Appl. Remote Sens.*, **2**, 144–162, doi:10.1109/JSTARS.2009.2027443.

——, and Coauthors, 2012: Multi-scale meteorological conceptual analysis of observed active fire hotspot activity and smoke optical depth in the Maritime Continent. *Atmos. Chem. Phys.*, **12**, 2117–2147, doi:10.5194/acp-12-2117-2012.

——, and Coauthors, 2013: Observing and understanding the Southeast Asian aerosol system by remote sensing: An initial review and analysis for the Seven Southeast Asian Studies (7SEAS) program. *Atmos. Res.*, **122**, 403–468, doi:10.1016/j.atmosres.2012.06.005.

Salinas, S. V., B. N. Chew, and S. C. Liew, 2009: Retrievals of aerosol optical depth and Ångström exponent from ground-based Sun-photometer data of Singapore. *Appl. Opt.*, **48**, 1473–1484, doi:10.1364/AO.48.001473.

——, ——, J. Miettinen, J. R. Campbell, E. J. Welton, J. S. Reid, L. E. Yu, and S. C. Liew, 2013: Physical and optical characteristics of the October 2010 haze event over Singapore: A photometric and lidar analysis. *Atmos. Res.*, **122**, 555–570, doi:10.1016/j.atmosres.2012.05.021.

Sarvision, 2011. Impact of oil palm plantations on peatland conversion in Sarawak 2005–2010, 16 pp. [Available online at http://www.wetlands.org/Portals/0/publications/Report/Sarvision%20Sarawak%20Report%20Final%20for%20Web.pdf.]

Schell, B., I. J. Ackermann, H. Hass, F. S. Binkowski, and A. Ebel, 2001: Modeling the formation of secondary organic aerosol within a comprehensive air quality model system. *J. Geophys. Res.*, **106**, 28 275–28 293, doi:10.1029/2001JD000384.

Schroeder, W., E. Prins, L. Giglio, I. Csiszar, C. Schmidt, J. T. Morisette, and D. Morton, 2008: Validation of GOES and MODIS active fire detection products using ASTER and ETM+. *Remote Sens. Environ.*, **112**, 2711–2726, doi:10.1016/j.rse.2008.01.005.

See, S. W., R. Balasubramanian, and W. Wang, 2006: A study of the physical, chemical, and optical properties of ambient aerosol particles in Southeast Asia during hazy and nonhazy days. *J. Geophys. Res.*, **111**, D10S08, doi:10.1029/2005JD006180.

Shi, Y., J. Zhang, J. S. Reid, B. Holben, E. J. Hyer, and C. Curtis, 2011: An analysis of the Collection 5 MODIS over-ocean aerosol optical depth product for its implication in aerosol assimilation. *Atmos. Chem. Phys.*, **11**, 557–565, doi:10.5194/acp-11-557-2011.

Song, C. H., and Coauthors, 2008: An investigation into seasonal and regional aerosol characteristics in East Asia using model-predicted and remotely-sensed aerosol properties. *Atmos. Chem. Phys.*, **8**, 6627–6654, doi:10.5194/acp-8-6627-2008.

Stauffer, D. R., and N. L. Seaman, 1994: Multiscale four-dimensional data assimilation. *J. Appl. Meteor.*, **33**, 416–434, doi:10.1175/1520-0450(1994)033<0416:MFDDA>2.0.CO;2.

Stephens, G. L., and Coauthors, 2002: The *CloudSat* mission and the A-Train. *Bull. Amer. Meteor. Soc.*, **83**, 1771–1790, doi:10.1175/BAMS-83-12-1771.

Stockwell, W. R., P. Middleton, J. S. Chang, and X. Tang, 1990: The second generation regional acid deposition model chemical mechanism for regional air quality modeling. *J. Geophys. Res.*, **95**, 16 343–16 367, doi:10.1029/JD095iD10p16343.

Turk, F. J., and S. Miller, 2005: Toward improving estimates of remotely-sensed precipitation with MODIS/AMSR-E blended data techniques. *IEEE Trans. Geosci. Remote Sens.*, **43**, 1059–1069, doi:10.1109/TGRS.2004.841627.

——, and P. Xian, 2013: An assessment of satellite-based high resolution precipitation datasets for atmospheric composition studies in the Maritime Continent. *Atmos. Res.*, **122**, doi:10.1016/j.atmosres.2012.02.017.

Wang, J., and S. A. Christopher, 2006: Mesoscale modeling of Central American smoke transport to the United States: 2. Smoke radiative impact on regional surface energy budget and boundary layer evolution. *J. Geophys. Res.*, **111**, D14S92, doi:10.1029/2005JD006720.

——, ——, U. S. Nair, J. S. Reid, E. M. Prins, J. Szykman, and J. L. Hand, 2006: Mesoscale modeling of Central American smoke transport to the United States: 1. "Top-down" assessment of emission strength and diurnal variation impacts. *J. Geophys. Res.*, **111**, D05S17, doi:10.1029/2005JD006416.

——, and Coauthors, 2013: Mesoscale modeling of smoke transport over the Southeast Asian Maritime Continent: Interplay of sea breeze, trade wind, typhoon, and topography. *Atmos. Res.*, **122**, 486–503, doi:10.1016/j.atmosres.2012.05.009.

Wang, X, and Coauthors, 2010: WRF-Chem simulation of East Asian air quality: Sensitivity to temporal and vertical emissions distributions. *Atmos. Environ.*, **44**, 660–669, doi:10.1016/j.atmosenv.2009.11.011.

Welton, E., J. R. Campbell, J. D. Spinhirne, and V. Stanley Scott III, 2001: Global monitoring of clouds and aerosols using a network of micropulse lidar systems. *Tropospheric Aerosols and Clouds I*, U. Singh, T. Itabe, and N. Sugimoto, Eds., International Society for Optical Engineering (SPIE Proceedings, Vol. 4153), 151–158, doi:10.1117/12.417040.

Wiedinmyer, C., S. K. Akagi, R. J. Yokelson, L. K. Emmons, J. A. Al-Saadi, J. J. Orlando, and A. J. Soja, 2011: The Fire Inventory from NCAR (FINN): A high resolution global model to estimate the emissions from open burning. *Geosci. Model Dev.*, **4**, 625–641, doi:10.5194/gmd-4-625-2011.

Winker, D. M., and Coauthors, 2010: The *CALIPSO* mission: A global 3D view of aerosols and clouds. *Bull. Amer. Meteor. Soc.*, **91**, 1211–1229, doi:10.1175/2010BAMS3009.1.

Wong, M. S., X. Fei, J. Nichol, J. Fung, J. Kim, J. R. Campbell, and P. W. Chan, 2015: A multi-scale hybrid neural network retrieval model for dust storm detection, a study in Asia. *Atmos. Res.*, **158–159**, 89–106, doi:10.1016/j.atmosres.2015.02.006.

Xian, P., J. S. Reid, J. F. Turk, E. J. Hyer, and D. L. Westphal, 2009: Impact of modeled versus satellite measured tropical precipitation on regional smoke optical thickness in an aerosol transport model. *Geophys. Res. Lett.*, **36**, L16805, doi:10.1029/2009GL038823.

——, ——, S. A. Atwood, R. S. Johnson, E. J. Hyer, D. L. Westphal, and W. Sessions, 2013: Smoke aerosol transport patterns over the Maritime Continent. *Atmos. Res.*, **122**, 469–485, doi:10.1016/j.atmosres.2012.05.006.

Yin, Y., K. S. Carslaw, and G. Feingold, 2005: Vertical transport and processing of aerosols in a mixed-phase convective cloud and the feedback on cloud development. *Quart. J. Roy. Meteor. Soc.*, **131**, 221–245, doi:10.1256/qj.03.186.

Zhang, C., 2013: Madden–Julian oscillation: Bridging weather and climate. *Bull. Amer. Meteor. Soc.*, **94**, 1849–1870, doi:10.1175/BAMS-D-12-00026.1.

Zhang, J., and J. S. Reid, 2006: MODIS aerosol product analysis for data assimilation: Assessment of over-ocean level 2 aerosol optical thickness retrievals. *J. Geophys. Res.*, **111**, D22207, doi:10.1029/2005JD006898.

——, and ——, 2010: A decadal regional and global trend analysis of the aerosol optical depth using a data-assimilation grade over-water MODIS and Level 2 MISR aerosol products. *Atmos. Chem. Phys.*, **10**, 10 949–10 963, doi:10.5194/acp-10-10949-2010.

——, ——, D. L. Westphal, N. L. Baker, and E. J. Hyer, 2008: A system for operational aerosol optical depth assimilation over global oceans. *J. Geophys. Res.*, **113**, D10208, doi:10.1029/2007JD009065.

——, J. R. Campbell, J. S. Reid, D. L. Westphal, N. L. Baker, W. F. Campbell, and E. J. Hyer, 2011: Evaluating the impact of assimilating CALIOP-derived aerosol extinction profiles on a global mass transport model. *Geophys. Res. Lett.*, **38**, L14801, doi:10.1029/2011GL047737.

——, ——, E. J. Hyer, J. S. Reid, D. L. Westphal, and R. Johnson, 2014: Evaluating the impact of multisensor data assimilation on a global aerosol particle transport model. *J. Geophys. Res.*, **119**, 4674–4689, doi:10.1002/2013JD020975.

Zhang, Q., and Coauthors, 2009: Asian emissions in 2006 for the NASA INTEX-B mission. *Atmos. Chem. Phys.*, **9**, 5131–5153, doi:10.5194/acp-9-5131-2009.